Chemical Engineering Journal 508 (2025) 160899

Contents lists available at ScienceDirect

Chemical Engineering Journal

journal homepage: www.elsevier.com/locate/cej

Spiral-structured electrospun conductive conduits filled with aligned nanofibers for peripheral nerve regeneration

Jiahui Song [a,1], Siyuan Wu [b,1], Chenlong Liao [d,1], Zhengchao Yuan [a], Xiao Yu [a], Panpan Shang [c], Yihong Shen [a], Jie Cui [a], Jinglei Wu [a], Binbin Sun [a], Mohamed EL-Newehy [e], Meera Moydeen Abdulhameed [e], Shuo Zhang [b], Wenchuan Zhang [d,*], Shichao Jiang [b,*], Xiumei Mo [a,c,*]

[a] State Key Laboratory for Modification of Chemical Fibers and Polymer Materials, Shanghai Engineering Research Center of Nano-Biomaterials and Regenerative Medicine, College of Biological Science and Medical Engineering, Donghua University, Shanghai 201620, China
[b] Department of Orthopedics, Shandong Provincial Hospital Affiliated to Shandong First Medical University, Jinan 250021, China
[c] Institute of Biomaterials and Biomedicine, School of Food and Pharmacy, Shanghai Zhongqiao Vocational and Technical University, Shanghai 201514, China
[d] Department of Neurosurgery, Shanghai Ninth People's Hospital, Shanghai Jiao Tong University School of Medicine, Shanghai 200240, China
[e] Department of Chemistry, College of Science, King Saud University, P.O. Box 2455, Riyadh 11451, Saudi Arabia

ARTICLE INFO

Keywords:
Electrospinning
PEDOT
Conductive conduits
Nerve regeneration

ABSTRACT

Peripheral nerve injury usually results in motor and sensory impairments, with nerve guidance conduits (NGCs) representing a promising strategy to facilitate nerve regeneration. The recovery of peripheral nerve injury is critically influenced by the topographic guidance cues and electrical properties of NGCs. In this study, the combination of hydroxyethyl cellulose (HEC) and poly(3,4-ethylenedioxythiophene) (PEDOT) was used for the first time to enhance the conductivity of conduits. Through electrospinning, spiral-structured conductive PLCL/HEC-PEDOT NGCs filled with aligned nanofibers (F-P/H-P) were fabricated. These electrospun F-P/H-P NGCs exhibited superior electrical conductivity, which significantly enhanced the adhesion and proliferation of SCs and PC12 cells and further promoted the expression of S100 and NF200 proteins in combination with electrical stimulation. In vivo experiments utilizing sciatic nerve defect models revealed that the conductive F-P/H-P conduit significantly accelerated peripheral nerve regeneration, neovascularization, and functional recovery. This study demonstrates the potential of electrospun conductive NGCs filled with aligned nanofiber membranes (F-P/H-P) to promote peripheral nerve regeneration and functional restoration.

1. Introduction

Peripheral nerves are extensively distributed throughout the human body and serve as a critical communication link between the central nervous system and the rest of the body. Peripheral nerve injury (PNI) is a prevalent clinical disease, with over 5 million cases reported globally each year [1]. The current gold standard for treating PNI is autologous nerve transplantation, but this approach is significantly limited by donor site morbidity and suboptimal functional recovery [2,3]. Given these challenges, substantial research has focused on developing advanced nerve guidance conduits (NGCs) as an alternative strategy for nerve regeneration [4,5]. Traditional hollow NGCs have demonstrated regenerative potential but are limited in their suitability for large nerve defects, primarily due to the absence of biophysical cues and inadequate mechanical stability [6].

To address these limitations, researchers have developed NGCs with an inner layer of aligned nanofibers, which provide directional guidance for cell growth and axon regeneration [7]. The aligned spiral structure within NGCs increases the specific surface area, providing Schwann cells (SCs) with more adhesion points, thus enhancing cell adhesion and proliferation while offering additional guidance for nerve regeneration [8]. Additionally, the outer layer of random nanofiber serves a dual purpose: preventing scar tissue invasion and providing sustained mechanical support during the regeneration process [9]. The incorporation of electroconductive materials into NGCs has gained attention due to the sensitivity of nerve cells to electrical stimulation (ES), which promotes

* Corresponding authors.
E-mail addresses: Zhangwench88@sjtu.edu.cn (W. Zhang), mailjsc@163.com (S. Jiang), xmm@dhu.edu.cn (X. Mo).
[1] Jiahui Song, Siyuan Wu, and Chenlong Liao are co-first authors.

https://doi.org/10.1016/j.cej.2025.160899
Received 5 December 2024; Received in revised form 17 February 2025; Accepted 20 February 2025
Available online 21 February 2025

cell differentiation and axon regeneration [10]. While some studies have explored the application of external ES, others have demonstrated that intrinsic electrical signals generated by nerve cells can also achieve significant regenerative outcomes [11–13].

Numerous studies have demonstrated that the incorporation of electroconductive biomaterials into NGCs facilitates ES throughout the active proliferation state in vivo [14–16]. Among the conductive materials explored for neural tissue engineering, metals, carbon nanomaterials, and conductive polymers have been widely utilized. However, metal-based and carbon-based materials often face challenges such as inhomogeneous distribution and compromised mechanical properties due to excessive admixture [17]. In contrast, conductive polymers offer distinct advantages, including improved conductivity and mechanical strength, while avoiding these issues. Poly(3,4-ethylenedioxythiophene) (PEDOT) is notable for its superior conductivity and stability relative to polypyrrole (PPy) and polyaniline (PANi), making it a standout choice in the realm of conductive polymers [18–20]. Despite its excellent properties, PEDOT is insoluble in water and most organic solvents, limiting its practical application. To address this limitation, poly(styrene sulfonate) (PSS) has been employed as a dispersant to form a PEDOT:PSS polymer electrolyte. This complex consists of positively charged PEDOT and negatively charged PSS, enabling stable dispersion of PEDOT in solvents [21]. However, the use of PSS introduces additional challenges, including reduced electrical conductivity, long-term stability, and biocompatibility, which restrict its biological applications [22]. To overcome these limitations, alternative electronegative ligands, such as chondroitin sulfate, xanthan gum, and hyaluronic acid, have been investigated as potential replacements for PSS [23–25]. The negatively charged hydroxyl groups in hydroxyethyl cellulose (HEC) can form electrostatic interactions with the positively charged PEDOT [26]. Furthermore, to improve the degradability and biocompatibility of conductive biomaterials, heteroaromatic conductive segments of PEDOT have been combined with aliphatic chains of biodegradable polymers, such as poly (L-lactide-co-caprolactone) (PLCL) through ester linkages [27]. This approach enhances the performance of materials while meeting the requirements of neural tissue engineering applications.

In this study, degradable PLCL, biocompatible HEC, and highly conductive PEDOT were integrated into nanofibers by electrospinning, working synergistically with ES to influence nerve cell behavior and promote nerve regeneration in vivo, as illustrated in Scheme 1. NGCs filled with aligned conductive nanofibers were constructed to mimic the aligned structure and conductivity of neural axons, integrating both structural and electrical cues to synergistically promote nerve regeneration. The mechanical properties, conductivity, hydrophily, and degradation of PLCL/HEC (P/H), hollow PLCL/HEC-PEDOT (H-P/H-P), and filled PLCL/HEC-PEDOT (F-P/H-P) NGCs were systematically characterized. Then, the adhesion, proliferation, and differentiation of SCs and PC12 cells on the nanofibers were evaluated in vitro, both in the presence and absence of ES. Finally, the efficacy of these NGCs in promoting nerve regeneration and functional recovery was evaluated in rat models of sciatic nerve defects.

2. Results and discussion

2.1. Characterizations of NGCs

Isotropic and anisotropic bilayer nanofiber conduits were fabricated by electrospinning. SEM images revealed that each group of nanofibers exhibited excellent surface morphology, characterized by uniform and smooth fibers as well as interconnected pores (Fig. 1A and B). Statistical analysis of fiber diameters exhibited that the P/H-P group had smaller fiber diameters compared to the P/H group, a trend observed in both random and aligned layers (Fig. 1C and D). The incorporation of PEDOT enhanced the conductivity of the spinning solution, thereby exerting a stronger pull on the nanofibers under identical electric field conditions. Notably, while the P/H membrane failed to conduct sufficient electricity to illuminate an LED lamp, the P/H-P membrane demonstrated conductivity capable of lighting the bulb (Fig. 1E). Photographs of the P/H, H-P/H-P, and F-P/H-P conduits were presented in Fig. 1F. Mechanical tensile results of the three groups were shown in Fig. 1G. The tensile strength of the conduits with the conductive material PEDOT increased significantly, from 5.7 ± 0.6 to 9.3 ± 1.2 MPa. The P/H, H-P/H-P, and F-P/H-P NGCs can easily match the necessary mechanical thresholds of conduits for nerve repair applications [28]. Besides, the F-P/H-P conduits with aligned spiral structures showed better tensile strength than the H-P/H-P conduits (Fig. 1H). These findings indicated that the fabricated nerve conduits possessed the requisite mechanical properties for effective nerve repair, including the ability to prevent scar tissue invasion and supporting peripheral nerve regeneration.

The enclosed region in the cyclic voltammetry (CV) curves corresponds to the quantity of charge transferred through the sample during testing. A larger enclosed area indicated greater charge transfer within the sample, which was indicative of superior conductivity. The CV diagram of the samples reflected a larger charge area and an increase in electrical conductance of the P/H-P group in comparison to the P/H

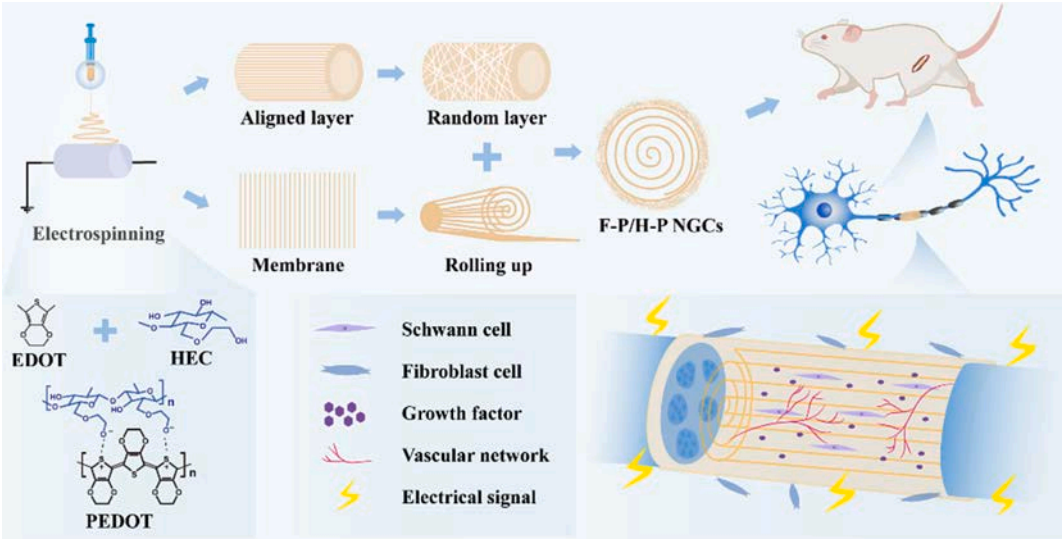

Scheme 1. Schematic illustration of conductive F-P/H-P NGCs for promoting nerve regeneration under ES.

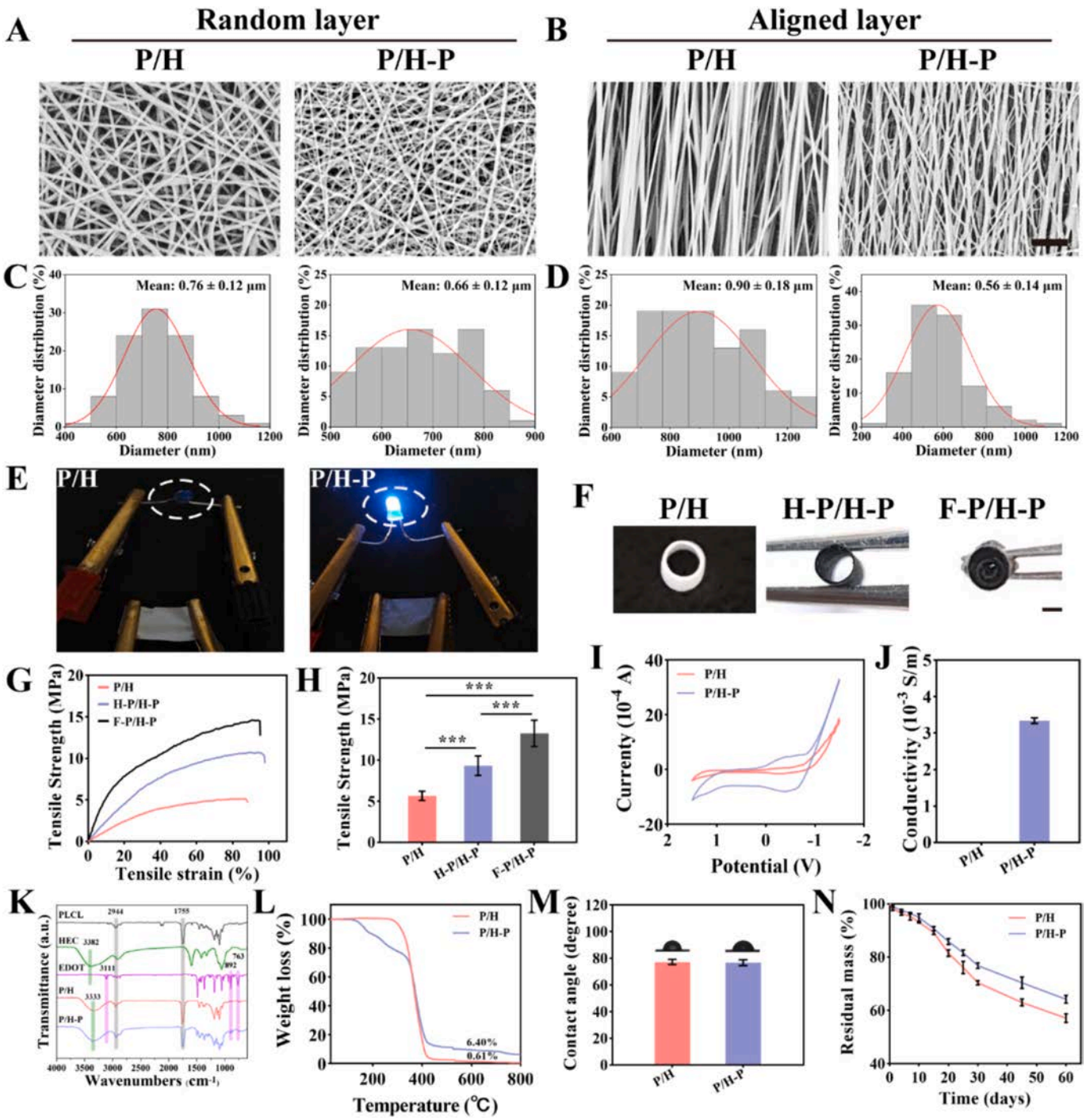

Fig. 1. Characterization of NGCs. SEM images of (A) random layers and (B) aligned layers of P/H and P/H-P nanofiber membranes. Scale bar: 10 μm. The statistics of nanofiber diameter of (C) random layers and (D) aligned layers of P/H and P/H-P membranes. (E) Conductivity observation of P/H and P/H-P membranes. (F) Photographs of P/H, H-P/H-P, and F-P/H-P conduits. Scale bar: 1 mm. (G) Stress–strain curves of P/H, H-P/H-P, and F-P/H-P conduits. (H) Tensile strength of different conduits. (I) CV curves of P/H and P/H-P membranes. (J) Conductivity of P/H and P/H-P membranes. (K) FTIR spectra, (L) TGA curves, (M) WCA, and (N) residual mass of P/H and P/H-P membranes. *p < 0.05, **p < 0.01, ***p < 0.001.

group (Fig. 1I, Table S2). The conductivity of the P/H-P membrane was measured at 3.34 ± 0.07 × 10^{-3} S cm^{-1}, while the P/H membrane was inconclusive due to its excessively high resistance (Fig. 1J). The above results confirmed that the addition of PEDOT markedly improved the conductivity of the material, thereby establishing a favorable electrophysiological microenvironment for damaged nerves.

FTIR test was employed to ascertain the molecular structure of materials and detect the polymerization of PEDOT. The FTIR spectra showed the ester group of 1756 cm^{-1} absorption peak and the methylene group of 2938 cm^{-1}, confirming the presence of PLCL [29]. Additionally, a hydroxy peak at 3429 cm^{-1} was observed, corresponding to the primary functional group of HEC [30]. The absorption peaks at 3111 cm^{-1} of the hydrocarbon bond on the thiophene ring and the peaks at 763 and 892 cm^{-1} of the unsaturated hydrocarbon bond disappeared following the polymerization of EDOT to PEDOT, providing clear evidence of successful PEDOT formation (Fig. 1K) [31,32]. In addition, the color change in the electrospinning solutions during EDOT polymerization, as shown in Fig. S1, was consistent with previous research [24].

These findings confirmed the efficient synthesis of conductive PEDOT.

The TGA results indicated that the residual mass at 800 °C was 0.6 % for the P/H membrane and 6.4 % for the P/H-P membrane (Fig. 1L). This difference indicated enhanced thermal stability of the P/H-P membrane due to the incorporation of PEDOT. As illustrated in Fig. 1M, WCA measurements showed values of 77.2 ± 2° for the P/H membrane and 76.7 ± 2.1° for the P/H-P membrane, indicating comparable hydrophilicity between the two types of membranes. The residual mass of the P/H membrane reached 57.1 %, while that of the P/H-P membrane was 64.1 % after 60 days of degradation, indicating favorable degradation properties for these materials (Fig. 1N).

Cultivation of SCs and PC12 cells with ES in vitro SCs play a crucial role in peripheral nerve repair, and numerous previous studies have demonstrated that ES efficiently facilitates the growth, adhesion, and myelination of SCs [33–35]. After one day of incubation, no significant differences in SCs proliferation were observed among various membranes (Fig. 2J). However, the proliferation of SCs on ES-P/H-P membranes was significantly promoted compared to P/H-P membranes after 3 days. After 5 days, the viability of SCs in the ES-P/H-P group surpassed all other groups, with the P/H-P group also outperforming the P/H and ES-P/H groups. Similar trends were observed in the proliferation of PC12 cells. According to Fig. 2K, PC12 cells cultured on ES-P/H-P membranes exhibited the highest cell viability after 4 and 7 days, with a significant difference compared to the P/H and P/H-P membranes. In conclusion, P/H-P membranes were determined to be the most effective for stimulating the growth of SCs and PC12 cells, especially when combined with ES.

S100 is a specific protein expressed by SCs that usually plays a neurotrophic role in peripheral nerves [36]. Furthermore, NF200 is a neurofilament protein specifically expressed in PC12 cells and serves as an important marker of mature axons [37]. To further investigate the interaction of nerve cells with P/H and P/H-P membranes with or without ES, immunofluorescence staining was performed to assess the specific expression of S100 and NF200 proteins in SCs and PC12 cells after 5 days of culture (Fig. 2A and B). Both S100 and NF200 proteins were expressed in all groups but at different levels of expression. Statistical analysis revealed that the ES-P/H-P group exhibited the highest proportion of positive expression for S100 and NF200, with the P/H-P group also showing significantly higher expression compared to the P/H and ES-P/H groups (Fig. 2H and I).

The Transwell assay was conducted to detect the longitudinal migration of PC12 cells after 24 h. Medium collected from the supernatant of SCs cultured for 5 days in different groups was used to culture PC12 cells, as illustrated in the schematic in Fig. 2E. Quantitative analysis indicated that the ES-P/H-P group exhibited the highest level of PC12 cell migration, with the P/H-P and ES-P/H groups also showing significantly enhanced migration compared to the P/H and control groups (Fig. 2C and F). Additionally, the ES-P/H-P group demonstrated the longest neurite length and the highest level of PC12 cell differentiation, while the P/H-P group also outperformed other groups in promoting differentiation of PC12 cells (Fig. 2G). Such obvious differences in the transwell assay experiment implied that the combination of P/H-P membranes with ES could indirectly recruit PC12 cells longitudinally and promote their differentiation. The indirect impact of scaffolds combined with ES on PC12 cells may be attributed to the increased secretion of potent nerve growth factors by SCs under the influence of ES, which in turn facilitated the differentiation and migration of PC12 cells [33,38].

SEM observations indicated that SCs and PC12 cells exhibited optimal adhesion on P/H-P materials, particularly in the ES-P/H-P group, which was consistent with the CCK-8 assay results. Additionally, SCs and PC12 cells grew along the aligned nanofibers, displaying more extended morphologies and larger adhesion areas on ES-P/H-P membranes (Fig. 2D). These findings suggested that the synergistic effects of PEDOT and ES played a positive role in inducing adhesion, proliferation, and migration of SCs and PC12 cells.

2.2. Gene expression analysis

The myelination of SCs plays a crucial role in the regeneration of injured nerves, prompting the examination of genes associated with different stages of SCs maturation. *NCAM* is expressed exclusively in immature SCs and diminishes as SCs mature, while the expression of *NGF* and *PMP22* progressively increases during SCs maturation [39]. Results demonstrated that the expression levels of *NGF* and *PMP22* genes were significantly upregulated, while *NCAM* expression was significantly attenuated in SCs cultured on P/H-P membrane with ES (Fig. 3A). These findings showed that the conductive P/H-P nanofiber scaffold combined with ES effectively enhanced SCs myelination.

The expression of specific genes in PC12 cells was analyzed to assess their differential stages under various conditions. *Nestin*, *βIII-Tubulin*, and *Map1b* serve as markers for different stages of neurogenesis: early-, mid-, and late-phase, respectively [40]. As shown in Fig. 3B, PC12 cells cultured on P/H-P membranes showed increased expression of *βIII-Tubulin* and *Map1b* genes after 5 days, even without ES, suggesting a higher proportion of cells in the middle and late stages of differentiation. Conversely, *Nestin* expression diminished in the ES-P/H-P group. Overall, P/H-P membranes under ES implied a significant potential to promote myelination and accelerate differentiation of PC12 cells (Fig. 3C).

Although the level of genes expression under ES has been detected, further research is required to elucidate the specific molecular mechanisms in neural cells. It is generally accepted that ES activates calcium ion channels in nerve cells, leading to an increase in intracellular calcium concentration and subsequent upregulation of genes associated with calcium ion signaling pathways during cell differentiation, ultimately maximizing the expression of various substances necessary for axon regeneration [41].

2.3. Subcutaneous implantation

The P/H, H-P/H-P, and F-P/H-P nerve conduits were implanted into the subcutaneous fascial layer of the back of rats for in vivo degradation studies (Fig. 4A). Photographs depicting each set of conduits 6 weeks post-implantation were illustrated in Fig. 4B. Degradation and tissue infiltration of these conduits were evident in the H&E staining images (Fig. 4C). Further analysis of the degree of tissue infiltration showed that the NGCs were partially replaced by neo-tissues, indicating good biocompatibility in vivo. The degree of tissue infiltration was significantly higher in the P/H and F-P/H-P conduits compared to the H-P/H-P conduits (Fig. 4D). Localized magnification of the interface between the tube wall and the subcutaneous tissue exhibited no significant inflammatory response in the blue box area. Immunofluorescence staining for CD68 in these three conduits confirmed no significant inflammatory cell infiltration, with consistent fluorescence intensity (Fig. 4E and 4F). Additionally, localized magnification of tissue infiltration revealed angiogenesis in all experimental groups within the red box area. Angiogenesis in these conduits was further analyzed by CD31 and α-SMA immunofluorescence staining (Fig. 4G). Statistical analysis indicated superior angiogenesis in the H-P/H-P and F-P/H-P conduits compared to the P/H group (Fig. 4H and 4I). The above findings indicated that all three categories of NGCs demonstrated in vivo degradation, favorable biocompatibility, and minimal inflammatory responses.

Histological analysis of regenerated sciatic nerves To evaluate the repair efficacy of the prepared nerve conduits in vivo, they were implanted into rat sciatic nerve defect models, with autografts serving as controls. All rats survived without complications at 6 and 12 weeks after surgery (Fig. 5A). Surgical implantation of NGCs in various groups was illustrated in Fig. 5B. H&E staining was initially employed to assess nerve repair in autografts, P/H, H-P/H-P, and F-P/H-P conduits. In this staining, chromatin and nucleic acids in the nuclei appeared purple-blue, while cellular and extracellular matrix components stained red, with positive staining indicating neurogenesis. Photographs of surgical implantation at 6 weeks were shown in Fig. S2A. H&E staining of

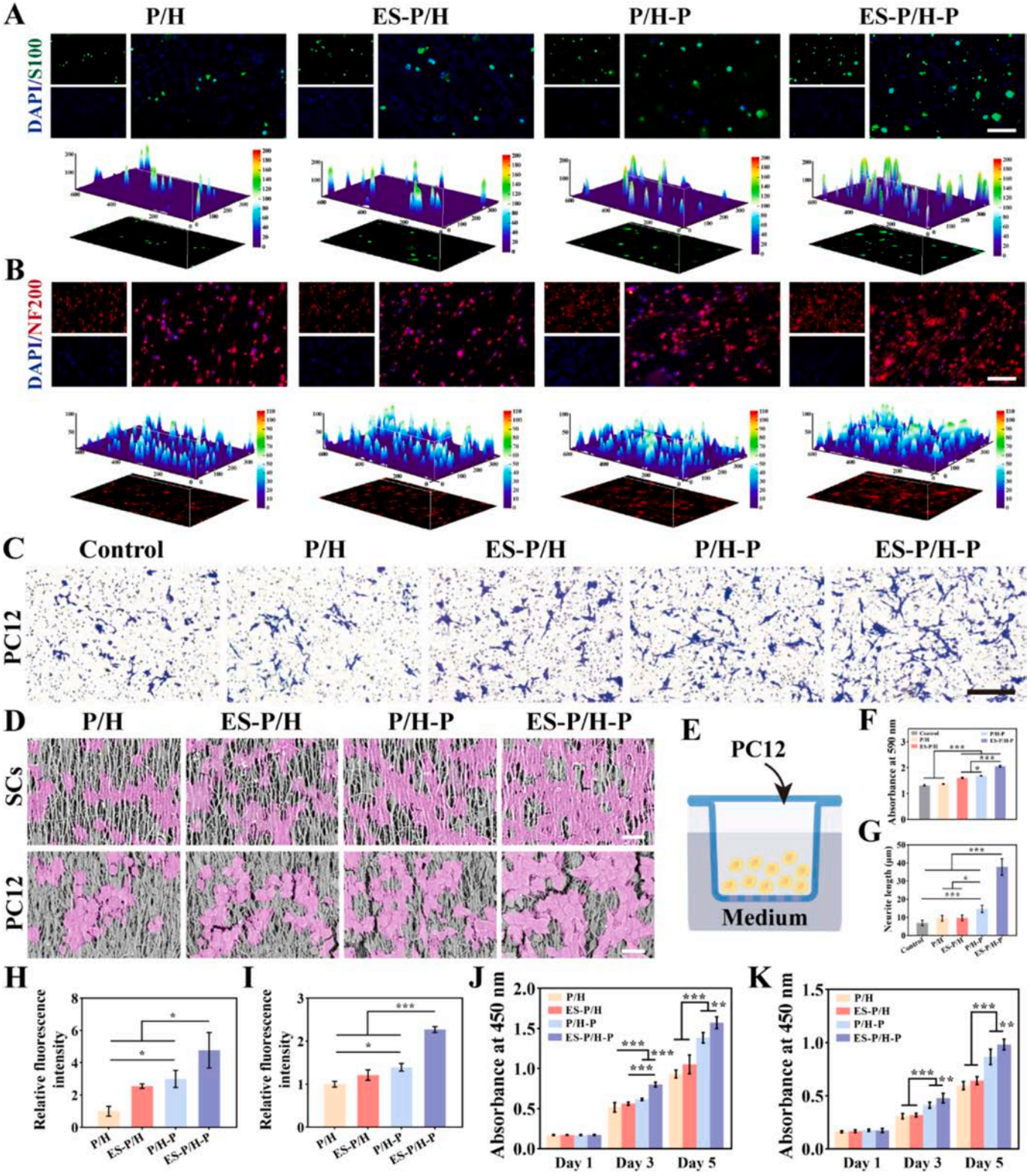

Fig. 2. Adhesion, proliferation, and migration of SCs and PC12 cells on P/H, ES-P/H, P/H-P and ES-P/H-P membranes. (A) Immunofluorescence staining of S100 (green) in SCs and (B) NF200 (red) in PC12 cells. Scale bar: 100 μm. (C) Crystal violet staining of migrated PC12 cells in different groups. Scale bar: 200 μm. (D) SEM images of SCs and PC12 cells adhesion on the surface of various membranes after 5 days of culture. Scale bar: 20 μm. (E) Schematic diagram of PC12 cells migration assay. (F) Calculation of the migration rate of PC12 cells. (G) Statistics of neurite length of PC12 cells in migration images. (H) Relative fluorescence intensity of S100 in SCs. (I) Relative fluorescence intensity of NF200 in PC12 cells. (J) Proliferation of SCs and (K) PC12 cells in various membranes. *$p < 0.05$, **$p < 0.01$, ***$p < 0.001$. (For interpretation of the references to color in this figure legend, the reader is referred to the web version of this article.)

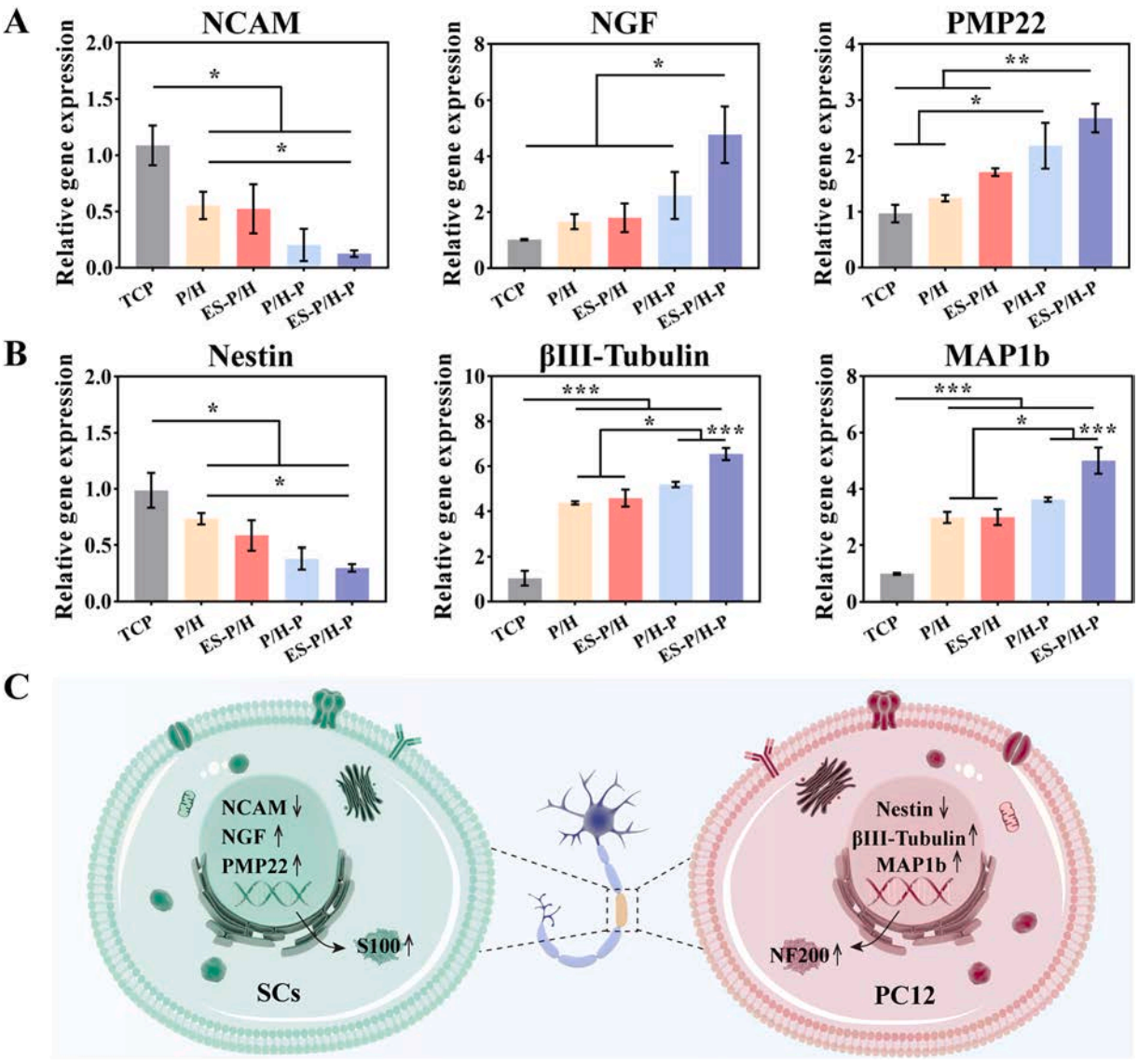

Fig. 3. Myelination gene expression of SCs and neurogenic gene expression of PC12 cells. (A) Transcription levels of myelination-related genes (*NCAM*, *NGF*, and *MP22*) in SCs cultured on various membranes after 5 days. (B) Transcription levels of neuron-specific genes (*Nestin*, *βIII-Tubulin*, and *MAP1b*) in PC12 cells cultured on various membranes after 5 days. (C) Schematic diagram of genes and proteins expression in SCs and PC12 cells. *p < 0.05, **p < 0.01, ***p < 0.001.

proximal cross section of each group revealed favorable growth trends at 6 weeks (Fig. S2B). After 12 weeks, regenerated nerves extended into all conduits (Fig. 5D). Notably, F-P/H-P conduits showed significantly higher positive H&E staining areas compared to H-P/H-P and P/H conduits, indicating superior nerve tissue regeneration. Detailed H&E staining of proximal, middle, and distal cross sections of the injured nerves was further observed for nerve tissue regeneration (Fig. 5C and 5E). Similarly, the F-P/H-P conduits showed tissue growth comparable to autografts at 12 weeks, with proximal and central regions displaying greater nerve extension and regeneration than distal regions. These results confirmed the critical role of topographic guidance cues provided by nerve conduits in directing nerve regeneration.

Intraneural microvessels are essential for nerve regeneration, creating a regenerative microenvironment by enabling material exchange and nutrient transport [42]. The presence of neovascularization containing erythrocytes was observed in magnified cross sections of distal regions of regenerating nerve tissue from all experimental groups, as highlighted by yellow arrows (Fig. 5E). To further assess angiogenesis, immunofluorescence staining for CD31 and α-SMA of the regenerated nerves was performed on the distal nerve segment at 12 weeks post-surgery (Fig. 5F and G). Areas positive for CD31 were indicative of new blood vessel formation, while double positive areas for CD31 and α-SMA were designated as mature vessels. Quantitative analysis revealed that CD31 fluorescence intensity in the H-P/H-P and F-P/H-P groups was comparable to autografts and significantly higher than in the P/H group, demonstrating enhanced neovascularization in the conductive and aligned nanofiber membrane-filled conduit (Fig. 5H). Moreover, α-SMA fluorescence intensity was higher in H-P/H-P and F-P/H-P conduits than in the P/H group, indicating a much better maturity of angiogenesis in the conduits that are both conductive and provide topographical guidance cues (Fig. 5I). Quantitative analysis of microvessel density and diameter (Fig. 5J and 5 K) revealed that the F-P/H-P group exhibited neovascularization capacity similar to that of the autograft group, with a significant increase in the number of newly formed blood vessels per unit area and vessel diameter compared to the P/H and H-P/H-P NGCs. These findings indicated that the F-P/H-P NGCs significantly promoted peripheral nerve tissue regeneration and angiogenesis, closely matching the performance of autografts. Thus, conductive materials and topographically guided cues promote peripheral nerve regeneration, in part, by facilitating intraneural angiogenesis for material exchange and

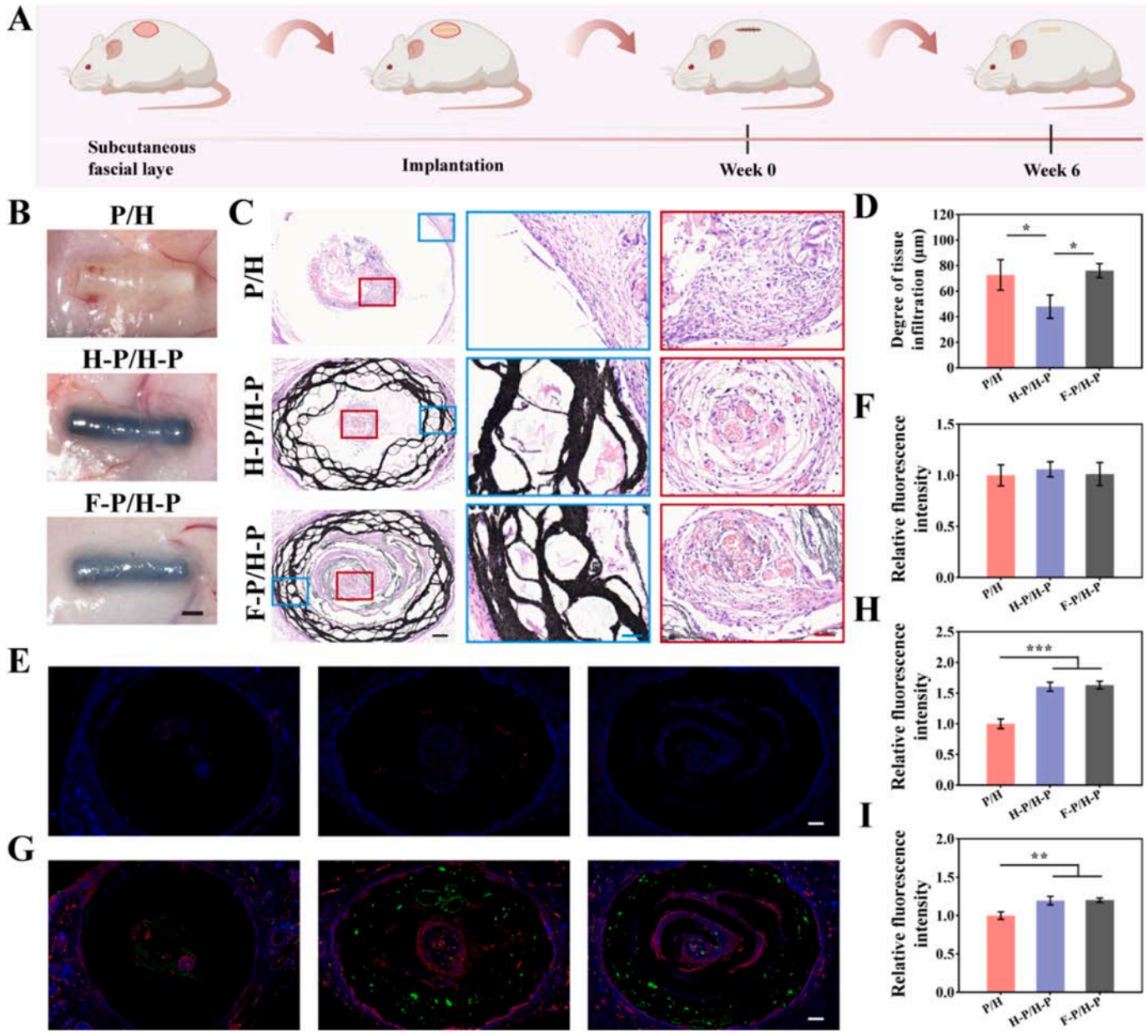

Fig. 4. Subcutaneous implantation of different conduits. (A) Schematic of subcutaneous implantation. (B) Photographs of the conduits after 6 weeks. Scale bar: 20 mm. (C) H&E staining of subcutaneous implantation cross sections of conduits after 6 weeks. Scale bar: 200 μm, 50 μm. (D) Quantitative analysis of the degree of tissue infiltration. (E) Immunofluorescence staining for CD68 of conduits after 6 weeks. Scale bar: 200 μm. (F) Quantitative analysis of CD68 relative fluorescence intensity. (G) Immunofluorescence staining for CD31 (green), α-SMA (red), and nuclei (blue). Scale bar: 200 μm. (H) Quantitative analysis of CD31 relative fluorescence intensity. (I) Quantitative analysis of α-SMA relative fluorescence intensity. *$p < 0.05$, **$p < 0.01$, ***$p < 0.001$. (For interpretation of the references to color in this figure legend, the reader is referred to the web version of this article.)

nutrient transport. Further studies are still needed to fully elucidate the underlying mechanisms.

2.4. Immunofluorescence staining of regenerated nerves

Immunofluorescence staining of longitudinal sections of regenerated nerves at 12 weeks after surgery revealed that S100 and NF200 expression in all groups, which was indicative of successful myelination and extension of nascent axons (Fig. 6A). The positive area and fluorescence intensity of S100 and NF200 were lower in the P/H group compared to the H-P/H-P and F-P/H-P groups, suggesting limited myelination and axon extension (Fig. 6B and C). Additionally, the staining results of the H-P/H-P and F-P/H-P groups demonstrated that conductivity and topographic guidance could promote myelination and axon regeneration. The fluorescence intensity and positive area of S100 and NF200 in the F-P/H-P group closely resembled those in the autologous transplantation group, with extensive yellow areas formed by overlapping red and green staining, representing the wrapping of axons by SCs.

2.5. Functional evaluation of the regenerated sciatic nerve

As the gastrocnemius muscle is innervated by the sciatic nerve, its atrophy reduction reflects sciatic nerve motor function recovery. Therefore, gross views and histological analysis of the gastrocnemius muscle were obtained 12 weeks post-surgery. Compared to the contralateral side, significant atrophy of the injured gastrocnemius muscle was observed in the P/H group as shown in Fig. 7A, while the autograft, H-P/

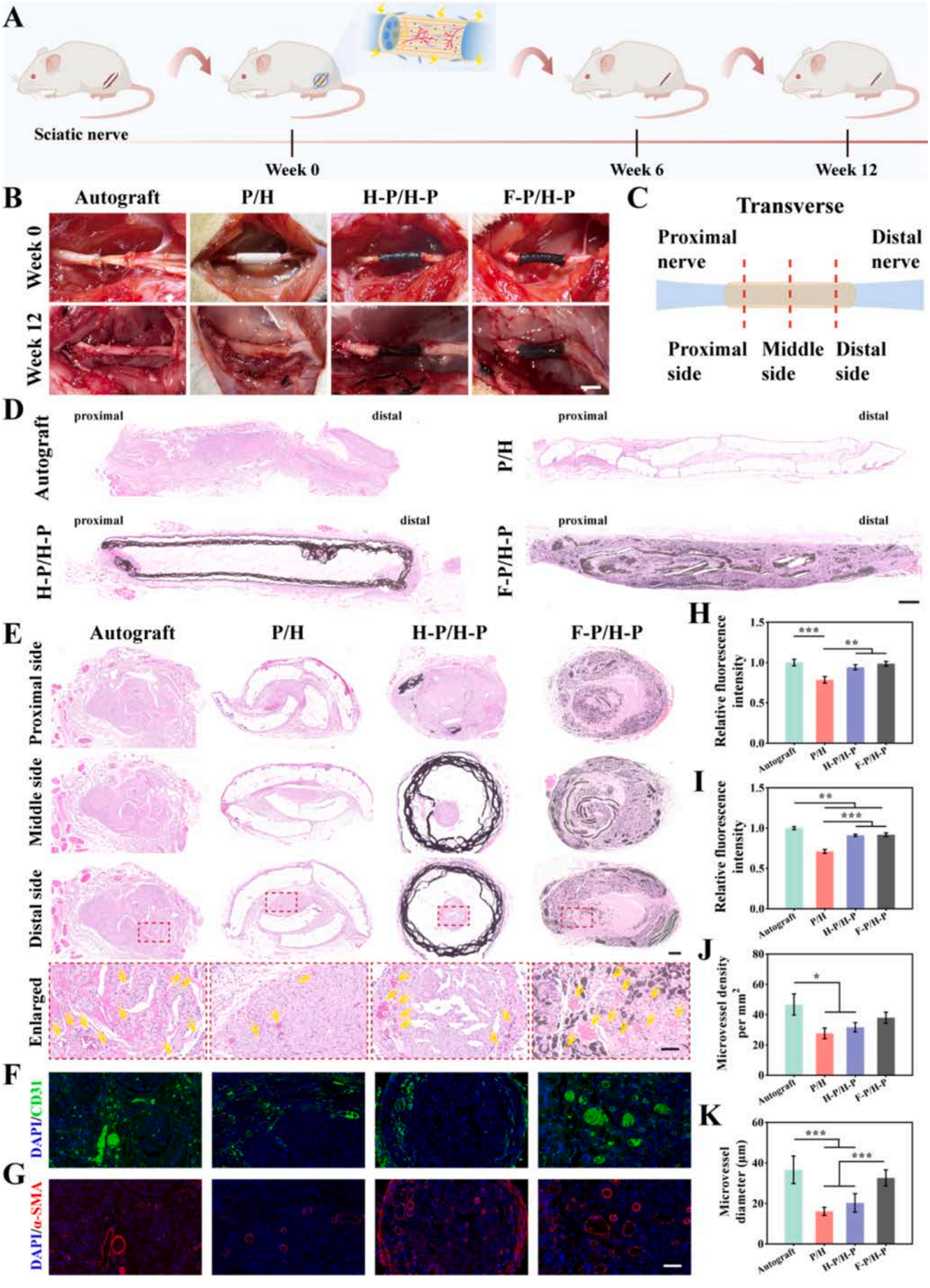

(caption on next page)

Fig. 5. Histological morphological assessment of autologous transplantation, P/H, H-P/H-P, and F-P/H-P conduits. (A) Schematic diagram of NGCs transplantation. (B) Photographs of surgical implantation. Scale bar: 0.5 cm. (C) Schematic illustration for tested transverse areas of nerves. (D) H&E staining images of longitudinal sections of regenerated nerve tissue at 12 weeks. Scale bar: 500 μm. (E) Cross sections of proximal, middle, and distal regenerated nerves at 12 weeks stained with H&E. Scale bar: 200 μm. Scale bar: 50 μm. Yellow arrows indicate neovascularization. (F) Immunofluorescence staining for CD31 (green) and nuclei (blue). Scale bar: 50 μm. (G) Immunofluorescence staining for α-SMA (green) and nuclei (blue). Scale bar: 50 μm. (H) Quantitative analysis of CD31 relative fluorescence intensity. (I) Quantitative analysis of α-SMA relative fluorescence intensity. (J) Microvascular density and (K) diameter calculated based on different groups. *$p < 0.05$, **$p < 0.01$, ***$p < 0.001$. (For interpretation of the references to color in this figure legend, the reader is referred to the web version of this article.)

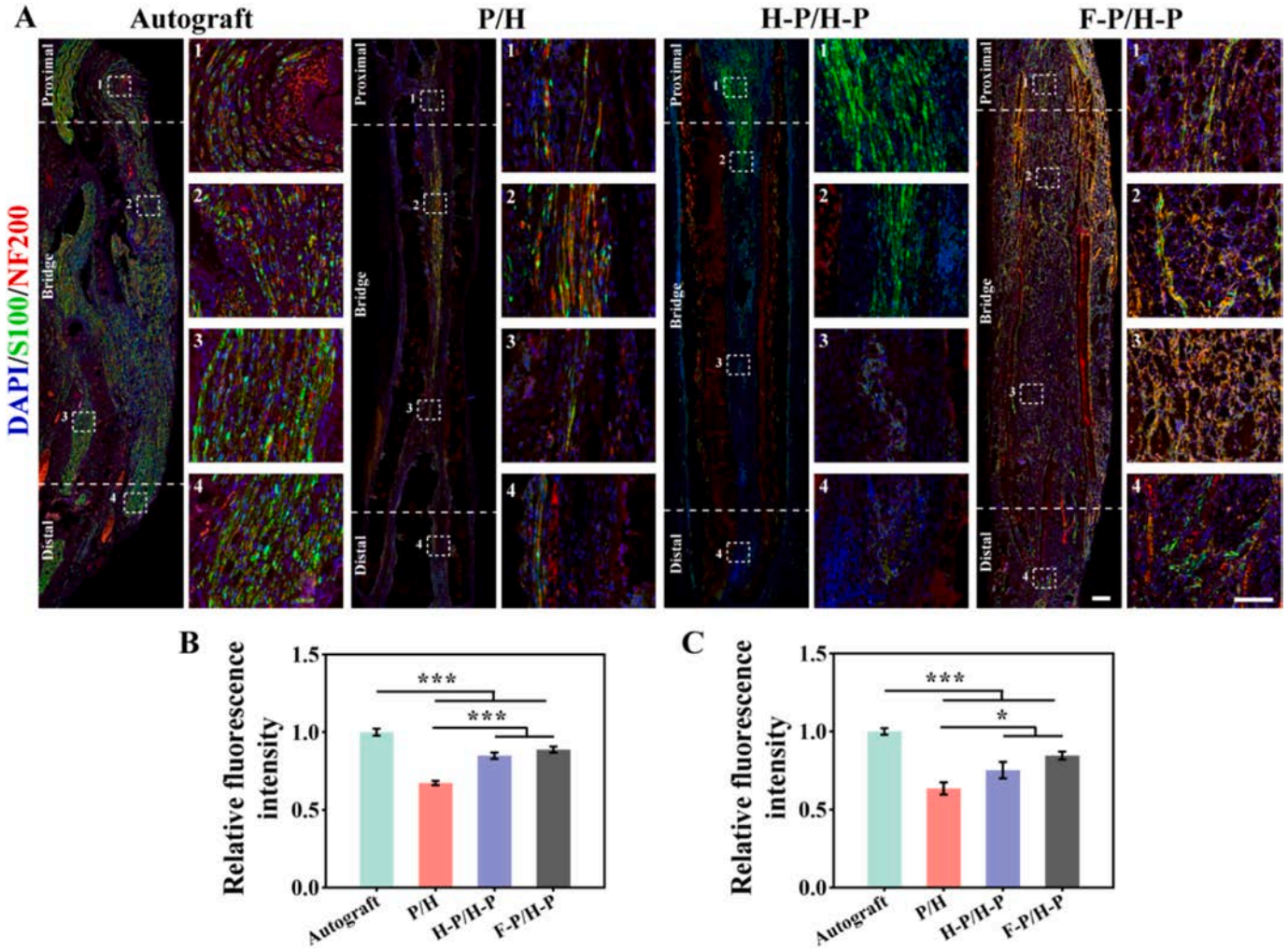

Fig. 6. Immunofluorescence staining of autologous transplantation, P/H, H-P/H-P, and F-P/H-P conduits at 12 weeks. (A) Immunofluorescence staining images of longitudinal sections of S100 (green), NF200 (red), and nuclei (blue). Scale bar: 200 μm (low magnification) and 100 μm (high magnification). (B) Relative fluorescence intensity of S100. (C) Relative fluorescence intensity of NF200. (For interpretation of the references to color in this figure legend, the reader is referred to the web version of this article.)

H-P, and F-P/H-P groups exhibited less atrophy. Quantitative analysis confirmed no difference in the wet weight ratio of the gastrocnemius muscle between the autograft and F-P/H-P groups, both significantly higher than the P/H group (Fig. 7E). The diameter and area of muscle fibers were evaluated by Masson's trichrome staining (Fig. 7B). The results indicated that the muscle fiber diameter and average area in the F-P/H-P group most closely resembled those in autologous transplantation group, followed by the H-P/H-P group (Fig. 7F and 7G). To further assess the restoration of neural function, SFI was calculated based on rat footprints (Figs. 7C and S3A). At 6 weeks, SFI values in the autograft and F-P/H-P groups showed a significant increase compared to the P/H group (Fig. S3C). There was no significant difference in the SFI between the autograft and F-P/H-P groups, and both were notably higher than those in the P/H and H-P/H-P groups at 12 weeks (Fig. 7H).

Besides, electrophysiological tests were conducted to assess the functional restoration of electrical conduction at 6 and 12 weeks post-surgery (Figs. S3B and 7D). At 6 weeks after implantation, CMAP amplitude and NCV in the autograft group were significantly superior to other experimental groups. Additionally, the F-P/H-P group exhibited better outcomes than the P/H group, with no discernible difference from the H-P/H-P group (Fig. S3D and S3E). At 12 weeks, the amplitude results of CMAP indicated no significant difference between the F-P/H-P and autograft groups, with both the F-P/H-P and H-P/H-P groups surpassing the P/H group (Fig. 7I). NCV in the F-P/H-P and H-P/H-P groups was faster than in the P/H group, and no significant difference was observed (Fig. 7J). These findings indicated that F-P/H-P conduits significantly improved the restoration of sciatic nerve conductivity and showed comparable outcomes to autologous transplantation as the duration of implantation increased from 6 to 12 weeks. Collectively, F-P/H-P conduits effectively facilitated functional restoration of injured sciatic nerves.

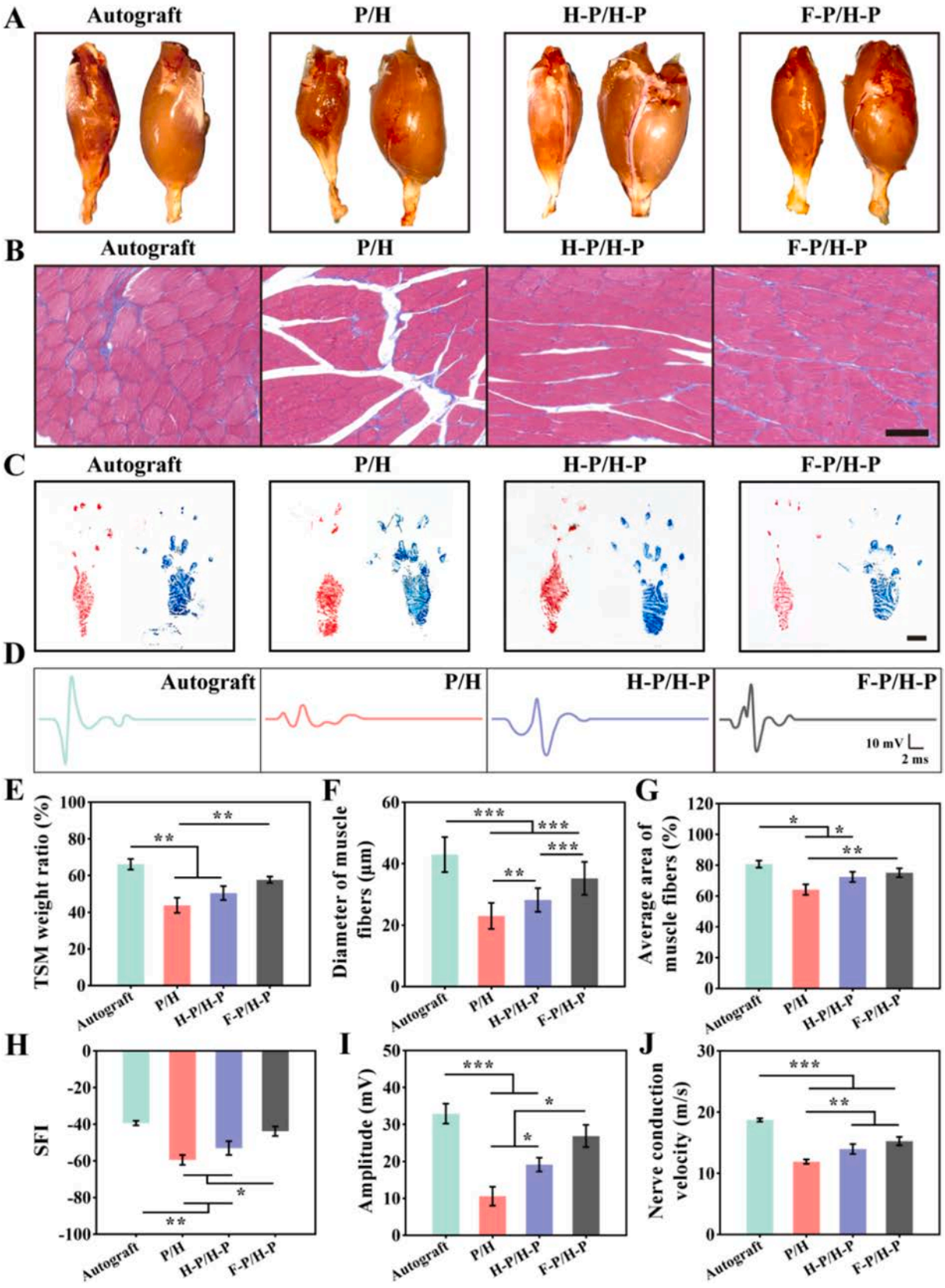

Fig. 7. Functional evaluation and the restoration of nerve conductivity at 12 weeks post-implantation. (A) Photographs of gastrocnemius muscles from both hind limbs. (B) Representative images of cross sections of gastrocnemius muscles stained with Masson's trichrome. Scale bar: 100 μm. (C) Photographs of footprints. Scale bar: 0.5 cm. (D) Representative CMAP recordings in the autograft, P/H, H-P/H-P, and F-P/H-P groups at the injury site. (E) Quantification of the TSM wet weight ratios of gastrocnemius muscles. (F) Quantification of the diameter of gastrocnemius muscles. (G) Quantification of the average area of muscle fibers. (H) Quantification of the SFI of hind paws. Quantification of (I) CMAP amplitude and (J) nerve conduction velocity in the indicated groups. *p < 0.05, **p < 0.01, ***p < 0.001.

3. Conclusion

Overall, this study systematically highlighted the synergistic benefits of combining conductive materials with biomimetic structural features. Advanced spiral conductive F-P/H-P NGCs filled with aligned nanofiber membranes were fabricated to effectively facilitate the complex processes of nerve repair and functional restoration. In vitro experimental results demonstrated that the excellent electrical conductivity of F-P/H-P NGCs significantly promoted the adhesion and proliferation of SCs and PC12 cells. This cellular response contributed to the improvement of nerve regeneration and function recovery. The results proved the advantages of using conductive conduits filled with aligned nanofibers for nerve repair. Such designs effectively mimic the biophysical cues inherent in natural peripheral nerves, promoting an environment conducive to nerve regeneration. Consequently, F-P/H-P NGCs are capable of bridging nerve transections and provide a promising alternative for peripheral nerve repair.

4. Materials and methods

4.1. Materials

The poly (L-lactide-co-caprolactone) (PLCL, LA: CL = 50:50, IV: 1.76 dl g^{-1}) was provided by Jinan Daigang Co., Ltd. (Jinan, China). 1,1,1,3,3,3-hexafluoro-2-propanol (HFIP, 920–66-1) was purchased from Shanghai Darui Fine Chemical Co., Ltd. (Shanghai, China). 3,4-ethylenedioxythiophene (EDOT, 126213–50-1) and ferric nitrate (7782–61-8) were obtained from Adamas-beta (Basel, Switzerland). Ammonium persulphate (APS, 10002616) was bought from China National Pharmaceutical Group (Shanghai, China). Schwann cells (SCs) and PC12 cells were provided by the Institute of Biochemistry and Cell Biology (Shanghai, China).

4.2. Fabrication of different NGCs

The P/H spinning solution was synthesized by dissolving hydroxyethyl cellulose (HEC) (0.1 g) in distilled water (1 mL) under magnetic stirring (500 rpm, 25°C) for 2 h. This solution was then gradually infused into HFIP (9 mL) under stirring at a high speed (800 rpm, 25°C) for 2 h to ensure solvent homogeneity. Subsequently, PLCL (0.6 g) was dissolved in the mixed solution through continuous agitation (500 rpm) for 12 h at 25°C. For the conductive P/H-P formulation, HEC (0.1 g) was dissolved in distilled water (1 mL). Then, APS (0.02 g) as a catalyst and ferric nitrate (0.02 g) as an oxidizing agent were added to the mixed solution. This mixture was then slowly added dropwise to HFIP (9 mL) while stirring at 800 rpm at room temperature. Then, EDOT (0.2 g) and PLCL (0.6 g) were added to the mixed solution followed by 24 h magnetic stirring to ensure complete polymerization. The P/H, H-P/H-P, and F-P/H-P conduits were prepared by electrospinning (Yongkang Leye Technology Development Co., Ltd. SS-3556H, Beijing, China). During electrospinning, solutions were dispensed through a syringe at 1 mL h^{-1}. A voltage of 12 kV was applied to the 20 G needle. Random nanofibers were collected on a rotating collector at 200 rpm to produce P/H conduits. The H-P/H-P conduits were constructed by collecting random nanofibers on a rotating collector at 200 rpm and aligned nanofibers at 2800 rpm, respectively. The P/H-P spinning solution was additionally spun into an aligned nanofiber membrane, which was cut into rectangular pieces measuring 1 cm × 0.6 cm (length × width) and then crimped into the H-P/H-P hollow conduit to form an internally filled F-P/H-P conduit with a spiral structure.

4.3. Characterization of NGCs

4.3.1. SEM analysis

After being sputter-coated with a nanometer-scale gold layer to enhance surface conductivity, the samples pasted on the sample tables with conductive glue were observed with Field Emission Scanning Electron Microscope (SEM, Hitachi TM-1000, Japan). The diameter distribution of the nanofibers were quantified from SEM micrographs (n = 100 fibers per sample) sing ImageJ software.

4.3.2. Mechanical testing

Mechanical properties were obtained using a universal testing machine (HY-940FS, China). Stress–strain curves were generated at a 5 mm/min strain rate with a 20 N extensometer. Before testing, conduit diameters were measured with a micrometer. Six samples were tested per group to ensure statistical significance.

4.3.3. Conductivity testing

Cyclic voltammetry (CV) test was carried out using an electrochemical workstation model CHI 760E produced by Shanghai Chenguang Instrument Co., Ltd. P/H or P/H-P nanofiber membranes (10 mm × 10 mm) served as the working electrode, with a saturated calomel electrode (SCE) as the reference electrode and a platinum electrode as the counter electrode. The electrolyte solution was 0.1 mol/L phosphate buffer solution (PBS) at pH 7.4. The CV is scanned at a potential of 0.4 to 1.2 V at a scanning rate of 100 mV/s in an electrolyte solution of deionized water.

The conductivity of each membrane was determined in dry conditions using a digital multimeter (8901S, Chenzhou Island Industrial Co., Ltd, Shenzhen, China). The cross-sectional area of the electrospinning membrane was determined by measuring its width and thickness with vernier calipers, and the conductivity (σ) was calculated from the equation (1):

$$\sigma = \frac{L}{AR}$$

R was the resistance of the membrane in "MΩ"; L was the distance between the two electrodes in "cm"; A was the cross-sectional area of the membrane in "cm^{2}". Six samples were tested per group.

4.3.4. Physiochemical properties

Specimens were scanned by Attenuated Total Reflection-Fourier Transform Infrared Spectroscopy (ATR-FTIR, Nicolet Instrument, Madison, USA) in the wavenumber range of 4000 to 600 cm^{-1}.

4.3.5. Thermostability

The thermostability of nanofiber membranes was evaluated by a thermogravimetric analyzer (TGA, TGA8000, Shanghai, China). Powdered samples were placed into crucibles, and some parameter settings were then made for the instrument.

4.3.6. Hydrophilicity testing

The samples were cut into 10 × 40 mm and pasted to glass sheets placed on the observation table for the water contact angle (WCA) test using an optical contact angle measuring instrument (OCA40, Dataphysics, Germany). The contact angle was recorded 5 s after the water droplets contacted the nanofibers, and the average of multiple measurements was taken.

4.3.7. Degradation of conduits

The P/H and P/H-P membrane samples were immersed in PBS at 37 ℃ in a incubator shaker (Thermo Fisher Scientific, USA). At predetermined time points (1, 4, 7, 10, 15, 20, 25, 30, 45, and 60 days), samples were freeze-dried and weighed to determine the weight loss ratio. Three samples were tested at each time point.

4.4. Cell culture and studies

4.4.1. Cell viability assessment

Prior to cell seeding, P/H and P/H-P membranes were sterilized using ultraviolet irradiation for 6 h per side. SCs and PC12 cells were

separately plated onto the membranes at a density of 1×10^5 cells/mL. SCs were cultured in Dulbecco's modified Eagle medium (DMEM) supplemented with 10 % fetal bovine serum and 1 % penicillin–streptomycin. PC12 cells were cultured in Roswell Park Memorial Institute (RPMI)-1640 medium containing 10 % donor horse serum, 5 % fetal bovine serum, and 1 % penicillin–streptomycin. After 24 h of initial culture, cells were exposed to ES with 100 mV potential for 1 h daily using a direct current power supply (HSPY-36–03, China). Besides, parallel control groups were cultured under identical conditions without ES. The proliferation of SCs and PC12 cells was assessed by CCK-8 assay (C0038, Beyotime, China) at 1, 3, and 5 days. Briefly, CCK-8 solution at a concentration of 100μL mL^{-1} was added into wells and incubated for 1 h.

4.4.2. PC12 cells migration and differentiation assessment

SCs were seeded on different scaffolds at a density of 2.0×10^4 per well, and ES was applied to the corresponding scaffolds. The culture medium of the corresponding cells was then collected for subsequent experiments. Transwell cell culture assay was performed using transwell inserts (Corning, USA). For the transwell migration assay, PC12 cells (2.0×10^4 per well) were seeded in the upper chambers of transwell inserts (Corning, USA), while the conditioned medium from SCs was added to the lower chambers. The lower chambers of the transwell inserts for each experimental group were supplemented with 2.5 % FBS, while the normal medium (5 % fetal bovine serum and 1 % double antibody) served as the control. After 24 h of incubation, PC12 cells in the upper chamber were stained with crystal violet (Biosharp, China) for 10 min and observed under a reflection microscope. PC12 cells with neurite lengths exceeding their cell body diameters were selected for neurite length analysis [43]. The lengths of the neurites were measured by ImageJ.

4.4.3. Gene expression analysis

Total mRNA was extracted from SCs and PC12 cells using a total RNA extraction kit (Novoprotein, China). RNA concentration and purity were determined spectrophotometrically (NanoDrop 2000, Thermo Fisher, USA) with A260/A280 ratios between 1.8–2.0. Then, cDNA synthesis was performed by a reverse transcription kit (Novoprotein, China). Real-time qPCR (RT-qPCR) was performed using LightCycler 480 SYBR Green Master Mix (Takara, Japan). Results were collected after repeating all experiments three times and calculated using the $2^{-\Delta\Delta Ct}$ method. Table S1 displayed the primers for each gene.

4.4.4. Cell immunofluorescence (IF) staining

Cells were fixed with 4 % paraformaldehyde (Sigma-Aldrich, USA) for 30 min after 5 days of culture. Samples were incubated with 0.1 % Triton X-100 (Sigma-Aldrich, USA) and 6 % BSA (Beyotime, China) for 1 h after washing with PBS. Subsequently, primary antibodies against S100 (1:200; Solarbio, China) and NF200 (1:200; Solarbio, China) were applied overnight at 4 °C. After washing with PBS, samples were incubated with the corresponding secondary antibodies of fluorescein isothiocyanate (FITC)-labeled goat anti-mouse IgG (1:200; Solarbio, China) and Cyc3-labeled goat anti-mouse IgG (1:200; Solarbio, China) for 1 h at 37 °C in the dark. Ultimately, the nuclei were stained with DAPI (1:200; Sigma-Aldrich, USA) for 10 min. Fluorescent images were visualized under a reflection microscope (DMi8, Leica, Germany).

4.5. In vivo studies

Ethical statement

All animal experiments were performed after the approvement from the Animal Experimental Ethics Committee of Shandong provincial hospital affiliated to Shandong first medical university (No.2024–077) and complied with the requirements of the National Institutes of Health Guide for the Care and Use of Laboratory Animals.

4.5.2. Subcutaneous implantation

Adult male Sprague-Dawley (SD) rats (8 weeks old, 200–250 g) were used for subcutaneous implantation experiments. P/H, H-P/H-P, and F-P/H-P NGCs were implanted into the subcutaneous fascial layer of rats. After 6 weeks post-implantation, the NGCs were excised from the local fascia layers for subsequent histological and morphological analysis.

4.5.3. Animal model and transplantation

Adult male SD rats (8 weeks old, 200–250 g) were used to establish a sciatic nerve defect model. Rats were randomly divided into four experimental groups (n = 6 per group): the autograft group, the P/H conduit graft group, the H-P/H-P conduit graft group, and the F-P/H-P conduit graft group. Surgical procedures were performed under aseptic conditions following intraperitoneal administration of 2 % pentobarbital sodium (40 mg kg^{-1}). Subsequently, the skin and subcutaneous muscle of the left posterior femur were incised to expose the sciatic nerve, which was resected in a 10 mm segment to create the sciatic nerve defect model. In the autograft group, the 10 mm nerve gap was turned over and sutured with the nerve stumps. For the other groups, the respective conduits were used to bridge the 10 mm gap between the nerve stumps. All suturing was performed microscopically using 8–0 nylon thread, followed by wound closure with 4–0 nylon sutures. Rats were sacrificed at 6 and 12 weeks after surgery.

4.5.4. Gait analysis

The gait analysis was performed to evaluate the recovery of locomotor function at 6 and 12 weeks post-operation. During testing, animals were allowed to walk on a narrow track with the left hind paw (surgical side) coated with non-toxic red ink and the right hind paw (normal side) coated with blue ink. Paw prints were collected from three consecutive runs, and the calculation of sciatic nerve function index (SFI) was calculated using the following formula (2):

$$SFI = -38.3 \times \frac{E \times PL - N \times PL}{N} \times PL + 109.5 \times \frac{E \times TS - N \times TS}{N} \times TS + 13.3 \times \frac{E \times IT - N \times IT}{N} \times IT - 8.8$$

E: the experimental side; N: the normal side; PL: the length from the heel to the third toe; TS: the length from the first to the fifth toe; IT: the second toe to the fourth toe. In this study, SFI values range from −100 to 0, with −100 representing total motor sciatic nerve dysfunction.

4.5.5. Muscle weight ratio and histological assessment

The gastrocnemius muscles of both hind limbs were dissected and weighed at 6 and 12 weeks post-surgery to calculate the muscle weight ratio (experimental side/normal side). The cross-sectional morphology of the gastrocnemius muscle on the damaged side was examined by Masson's trichrome staining. Muscle fiber diameter and the percentage of muscle fibers were quantified using ImageJ software.

4.5.6. Electrophysiological assessment

After rats were anesthetized at 6 and 12 weeks after surgery, the damaged nerve and the ipsilateral gastrocnemius muscle were re-exposed. The bipolar hook stimulating electrode was positioned proximal to the reparative nerve. A receiving electrode was inserted into the ipsilateral gastrocnemius muscle, with a ground electrode placed subcutaneously in a superficial muscle layer. A portable biological-function experimental system (BL-420S, Tai Meng) was used to collect the compound muscle action potential (CMAP). Then CMAP peak amplitude and latency, and the nerve conduction velocity (NCV) were determined the electrophysiological data obtained from the recordings.

4.5.7. Nerve histological assessment

Regenerated nerve tissues were dissected and soaked into 4 % paraformaldehyde at 6 and 12 weeks. Cross and longitudinal sections were performed after embedding in paraffin, and nerve regeneration

was observed through staining with hematoxylin and eosin (H&E). For immunofluorescence staining, cross sections were blocked with 5 % BSA for 1 h at room temperature. Sections were incubated overnight at 4°C with primary antibodies against CD31 (1:200; Solarbio, China) and α-SMA (1:200 1:200; Solarbio, China), followed by corresponding secondary antibodies of fluorescein isothiocyanate (FITC)-labeled goat anti-mouse IgG (1:200; Solarbio, China) for CD31 and Cyc3-labeled goat anti-mouse IgG (1:200; Solarbio, China) for α-SMA. Besides, longitudinal sections were incubated with the primary antibodies of S100 (1:200; Solarbio, China) and NF200 (1:200; Solarbio, China) at 4 ℃ for 12 h, followed by secondary antibodies of FITC-labeled goat anti-mouse IgG (1:200; Solarbio, China) and Cyc3-labeled goat anti-mouse IgG (1:200; Solarbio, China). Nuclei were stained with DAPI (1:200; Solarbio, China). All sections were observed with a slide viewer after scanning with the digital case system.

4.6. Statistical analysis

The data obtained were expressed as mean ± standard deviation (mean ± SD). Data were analyzed by one-way analysis of variance (ANOVA) using GraphPad Prism and SPSS software. *$p < 0.05$ and **$p < 0.01$, and ***$p < 0.001$ were considered statistically significant.

CRediT authorship contribution statement

Jiahui Song: Data curation, Conceptualization. **Siyuan Wu:** Methodology. **Chenlong Liao:** Project administration. **Zhengchao Yuan:** Validation, Supervision. **Xiao Yu:** Resources. **Panpan Shang:** Software. **Yihong Shen:** Investigation. **Jie Cui:** Supervision. **Jinglei Wu:** Validation. **Binbin Sun:** Project administration. **Mohamed EL-Newehy:** Visualization. **Meera Moydeen Abdulhameed:** Validation. **Shuo Zhang:** Software. **Wenchuan Zhang:** Funding acquisition. **Shichao Jiang:** Project administration. **Xiumei Mo:** Investigation, Funding acquisition.

Declaration of competing interest

The authors declare that they have no known competing financial interests or personal relationships that could have appeared to influence the work reported in this paper.

Acknowledgements

This work was supported by the Fundamental Research Funds for the Central Universities (24D311703), Science and Technology Commission of Shanghai Municipality, China (20DZ2254900), Sino German Science Foundation Research Exchange Center, China (M-0263), China Education Association for International Exchange (2022181), National Natural Science Foundation of China (82271389,81801219), Natural Science Foundation of Shanghai (21ZR1438100), Taishan Scholars Program of Shandong Province (tsqn201812141), Shandong Provincial Natural Science Foundation (ZR2021MH004) and the Chenguang Program of Shanghai Education Development Foundation and Shanghai Municipal Education Commission (23CGB08). This project was also supported by Researchers Supporting Project Number (RSP2025R65), King Saud University, Riyadh, Saudi Arabia.

Appendix A. Supplementary data

Supplementary data to this article can be found online at https://doi.org/10.1016/j.cej.2025.160899.

Data availability

All data that support the findings of this study are included in the paper and the Supporting Information. Additional data related to this paper are available from the corresponding author upon reasonable request.

References

[1] W.A. Lackington, A.J. Ryan, F.J. O'Brien, Advances in nerve guidance conduit-based therapeutics for peripheral nerve repair, ACS Biomater. Sci. Eng. 3 (7) (2017) 1221–1235, https://doi.org/10.1021/acsbiomaterials.6b00500.
[2] S. Houshyar, A. Bhattacharyya, R. Shanks, Peripheral nerve conduit: materials and structures, Acs Chem. Neurosci. 10 (8) (2019) 3349–3365, https://doi.org/10.1021/acschemneuro.9b00203.
[3] R.B. Wu, L. Wang, F.Y. Chen, Y.M. Huang, J.M. Shi, X.F. Zhu, Y. Ding, X.C. Zhang, Evaluation of artificial nerve conduit and autografts in peripheral nerve repair in the rat model of sciatic nerve injury, Neurol. Res. 38 (5) (2016) 461–466, https://doi.org/10.1080/01616412.2016.1181346.
[4] C. Zhang, J. Gong, J. Zhang, Z. Zhu, Y. Qian, K. Lu, S. Zhou, T. Gu, H. Wang, Y. He, M. Yu, Three potential elements of developing nerve guidance conduit for peripheral nerve regeneration, Adv. Funct. Mater. 33 (40) (2023) 2302251, https://doi.org/10.1002/adfm.202302251.
[5] W. Zhou, M.S.U. Rahman, C. Sun, S. Li, N. Zhang, H. Chen, C.C. Han, S. Xu, Y. Liu, Perspectives on the novel multifunctional nerve guidance conduits: from specific regenerative procedures to motor function rebuilding, Adv. Mater. 36 (14) (2024) 2307805, https://doi.org/10.1002/adma.202307805.
[6] D. Grinsell, C.P. Keating, Peripheral nerve reconstruction after injury: a review of clinical and experimental therapies, BioMed Res. Int. 2014 (2014) 1–13, https://doi.org/10.1155/2014/698256.
[7] S.K. Vimal, N. Ahamad, D.S. Katti, A simple method for fabrication of electrospun fibers with controlled degree of alignment having potential for nerve regeneration applications, Mater. Sci. Eng. C Mater. Biol. Appl. 63 (2016) 616–627, https://doi.org/10.1016/j.msec.2016.03.008.
[8] H. Xia, Q. Chen, Y. Fang, D. Liu, D. Zhong, H. Wu, Y. Xia, Y. Yan, W. Tang, X. Sun, Directed neurite growth of rat dorsal root ganglion neurons and increased colocalization with Schwann cells on aligned poly(methyl methacrylate) electrospun nanofibers, Brain Res. 1565 (2014) 18–27, https://doi.org/10.1016/j.brainres.2014.04.002.
[9] A. Sierakowska-Byczek, J. Radwan-Pragłowska, Ł. Janus, T. Galek, K. Łysiak, M. Tupaj, D. Bogdał, Environment-friendly preparation and characterization of multilayered conductive PVP/Col/CS composite doped with nanoparticles as potential nerve guide conduits, Polymers 16 (7) (2024) 875, https://doi.org/10.3390/polym16070875.
[10] S. Shrestha, B.K. Shrestha, J. Lee, O.K. Joong, B.S. Kim, C.H. Park, C.S. Kim, A conducting neural interface of polyurethane/silk-functionalized multiwall carbon nanotubes with enhanced mechanical strength for neuroregeneration, Mater. Sci. Eng. C 102 (2019) 511–523, https://doi.org/10.1016/j.msec.2019.04.053.
[11] Z.Q. Huang, M.M. Sun, Y.Y. Li, Z.Z. Guo, H. Li, Reduced graphene oxide-coated electrospun fibre: effect of orientation, coverage and electrical stimulation on Schwann cells behavior, J. Mater. Chem. B 9 (11) (2021) 2656–2665, https://doi.org/10.1039/d1tb00054c.
[12] Y. Yang, X. Yin, H. Wang, W. Qiu, L. Li, F. Li, Y. Shan, Z. Zhao, Z. Li, J. Guo, J. Zhang, Y. Zhao, Engineering a wirelessly self-powered and electroconductive scaffold to promote peripheral nerve regeneration, Nano Energy 107 (2023), https://doi.org/10.1016/j.nanoen.2022.108145.
[13] J.L. Song, B.B. Sun, S. Liu, W. Chen, Y.Z. Zhang, C.Y. Wang, X.M. Mo, J.Y. Che, Y. M. Ouyang, W.E. Yuan, C.Y. Fan, Polymerizing pyrrole coated poly (l-lactic acid-co-ε-caprolactone) (PLCL) conductive nanofibrous conduit combined with electric stimulation for long-range peripheral nerve regeneration, Front. Mol. Neurosci. 9 (2016), https://doi.org/10.3389/fnmol.2016.00117.
[14] P. Sun, Y. Guan, C. Yang, H. Hou, S. Liu, B. Yang, X. Li, S. Chen, L. Wang, H. Wang, Y. Huang, X. Sheng, J. Peng, W. Xiong, Y. Wang, L. Yin, A bioresorbable and conductive scaffold integrating silicon membranes for peripheral nerve regeneration, Adv. Healthc. Mater. 12 (32) (2023), https://doi.org/10.1002/adhm.202301859.
[15] L.M. Ni, Z. Yao, Y.F. Zhao, T.F. Zhang, J. Wang, S.Y. Li, Z.B. Chen, Electrical stimulation therapy for peripheral nerve injury, Front. Neurol. 14 (2023), https://doi.org/10.3389/fneur.2023.1081458.
[16] J. Qian, Z. Lin, Y. Liu, Z. Wang, Y. Lin, C. Gong, R. Ruan, J. Zhang, H. Yang, Functionalization strategies of electrospun nanofibrous scaffolds for nerve tissue engineering, Smart Mater. Med. 2 (2021) 260–279, https://doi.org/10.1016/j.smaim.2021.07.006.
[17] F.N. Mo, Q. Li, G.J. Liang, Y.W. Zhao, D.H. Wang, Y. Huang, J. Wei, C.Y. Zhi, A self-healing crease-free supramolecular all-polymer supercapacitor, Adv. Sci. 8 (12) (2021), https://doi.org/10.1002/advs.202100072.
[18] G.B. Tseghai, D.A. Mengistie, B. Malengier, K.A. Fante, PEDOT:PSS-based conductive textiles and their applications, Sensors-Basel 20 (7) (2020), https://doi.org/10.3390/s20071881.
[19] M. Rahman, T. Mahady Dip, R. Padhye, S. Houshyar, Review on electrically conductive smart nerve guide conduit for peripheral nerve regeneration, J. Biomed. Mater. Res. Part A 111(12) (2023) 1916-1950, https://doi.org/10.1002/jbm.a.37595.
[20] Y. Han, M. Sun, X. Lu, K. Xu, M. Yu, H. Yang, J. Yin, A 3D printable gelatin methacryloyl/chitosan hydrogel assembled with conductive PEDOT for neural tissue engineering, Compos. Part B-Eng. 273 (2024), https://doi.org/10.1016/j.compositesb.2024.111241.

[21] H. Zhang, H. Wang, B. Wen, L. Lu, Y. Zhao, R. Chai, Ultrasound-responsive composited conductive silk conduits for peripheral nerve regeneration, Small Struct. 4 (9) (2023), https://doi.org/10.1002/sstr.202300045.
[22] D. Mantione, I. del Agua, W. Schaafsma, J. Diez-Garcia, B. Castro, H. Sardon, D. Mecerreyes, Poly(3,4-ethylenedioxythiophene):glycosaminoglycan aqueous dispersions: toward electrically conductive bioactive materials for neural interfaces, Macromol. Biosci. 16 (8) (2016) 1227–1238, https://doi.org/10.1002/mabi.201600059.
[23] S. Song, X. Liu, J. Huang, Z. Zhang, Neural stem cell-laden 3D bioprinting of polyphenol-doped electroconductive hydrogel scaffolds for enhanced neuronal differentiation, Biomater. Adv. 133 (2022), https://doi.org/10.1016/j.msec.2021.112639.
[24] C. Winters, F. Zamboni, A. Beaucamp, M. Culebras, M.N. Collins, Synthesis of conductive polymeric nanoparticles with hyaluronic acid based bioactive stabilizers for biomedical applications, Today Chem. 25 (2022), https://doi.org/10.1016/j.mtchem.2022.100969.
[25] I. del Agua, S. Marina, C. Pitsalidis, D. Mantione, M. Ferro, D. Iandolo, A. Sanchez-Sanchez, G.G. Malliaras, R.M. Owens, D. Mecerreyes, Conducting polymer scaffolds based on poly(3,4-ethylenedioxythiophene) and xanthan gum for live-cell monitoring, ACS Omega 3 (7) (2018) 7424–7431, https://doi.org/10.1021/acsomega.8b00458.
[26] T. Park, J. Jeong, Y.J. Kim, H. Yoo, Weak molecular interactions in organic composite dry film lead to degradable, robust wireless electrophysiological signal sensing, Adv. Mater. Interfaces 24 (2022), https://doi.org/10.1002/admi.202200594.
[27] S. Jadoun, U. Riaz, V. Budhiraja, Biodegradable conducting polymeric materials for biomedical applications: a review, Med. Devices Sens. 4 (1) (2020), https://doi.org/10.1002/mds3.10141.
[28] Q. Dong, X. Yang, X. Liang, J. Liu, B. Wang, Y. Zhao, C. Huselstein, X. Feng, Z. Tong, Y. Chen, Composite hydrogel conduit incorporated with platelet-rich plasma improved the regenerative microenvironment for peripheral nerve repair, ACS Appl. Mater. Interfaces 15 (20) (2023) 24120–24133, https://doi.org/10.1021/acsami.3c02548.
[29] Y. Xu, J.L. Wu, H.M. Wang, H.Q. Li, N. Di, L. Song, S.T. Li, D.W. Li, Y. Xiang, W. Liu, X.M. Mo, Q. Zhou, Fabrication of electrospun poly(L-lactide-co-ε-caprolactone)/collagen nanoyarn network as a novel, three-dimensional, macroporous, aligned scaffold for tendon tissue engineering, Tissue Eng. Part C Methods 19 (12) (2013) 925–936, https://doi.org/10.1089/ten.tec.2012.0328.
[30] L. Moradi, L. Witek, V. Vivekanand Nayak, A. Cabrera Pereira, E. Kim, J. Good, C.-J. Liu, Injectable hydrogel for sustained delivery of progranulin derivative Atsttrin in treating diabetic fracture healing, Biomaterials 301 (2023), https://doi.org/10.1016/j.biomaterials.2023.122289.
[31] Y.F. Xu, Y. Wang, J.J. Liang, Y. Huang, Y.F. Ma, X.J. Wan, Y.S. Chen, A hybrid material of graphene and poly (3,4-ethyldioxythiophene) with high conductivity flexibility, and transparency, Nano Res. 2 (4) (2009) 343–348, https://doi.org/10.1007/s12274-009-9032-9.
[32] D. Gülercan, İ. Gergin, A.S. Sarac, Preparation and electrochemical performances of graphene oxide/PEDOT and reduced graphene oxide/PEDOT nanofibers and nanocomposites, Fibers Polym. 19 (10) (2018) 2178–2187, https://doi.org/10.1007/s12221-018-8393-7.
[33] J. Wang, Y. Cheng, L. Chen, T. Zhu, K. Ye, C. Jia, H. Wang, M. Zhu, C. Fan, X. Mo, In vitro and in vivo studies of electroactive reduced graphene oxide-modified nanofiber scaffolds for peripheral nerve regeneration, Acta Biomater. 84 (2019) 98–113, https://doi.org/10.1016/j.actbio.2018.11.032.
[34] J. Song, J. Dong, Z. Yuan, M. Huang, X. Yu, Y. Zhao, Y. Shen, J. Wu, M. El-Newehy, M.M. Abdulhameed, B. Sun, J. Chen, X. Mo, Shape-persistent conductive nerve guidance conduits for peripheral nerve regeneration, Adv. Healthc. Mater. 13 (26) (2024) 2401160, https://doi.org/10.1002/adhm.202401160.
[35] Q. Liu, G.J. Liu, X.Q. Liu, M. Yang, S.Y. Xing, Y.W. Du, X.Y. Xiong, Synthesis of an electrospun PHA/RGO/Au scaffold for peripheral nerve regeneration: an in vitro study, Appl. Nanosci. 10 (3) (2020) 687–694, https://doi.org/10.1007/s13204-019-01130-1.
[36] M. Mata, D. Alessi, D.J. Fink, S100 is preferentially distributed in myelin-forming schwann-cells, J Neurocytol 19 (3) (1990) 432–442, https://doi.org/10.1007/Bf01188409.
[37] R. Posmantur, R.L. Hayes, C.E. Dixon, W.C. Taft, Neurofilament-68 and neurofilament-200 protein-levels decrease after traumatic brain injury, J. Neurotraum. 11(5) (1994) 533-545, https://doi.org/ 10.1089/neu.1994.11.533.
[38] J.H. Huang, Z.X. Ye, X.Y. Hu, L. Lu, Z.J. Luo, Electrical stimulation induces calcium-dependent release of NGF from cultured schwann cells, Glia 58 (5) (2010) 622–631, https://doi.org/10.1002/glia.20951.
[39] Y.B. Wu, L. Wang, B.L. Guo, Y.P. Shao, P.X. Ma, Electroactive biodegradable polyurethane significantly enhanced Schwann cells myelin gene expression and neurotrophin secretion for peripheral nerve tissue engineering, Biomaterials 87 (2016) 18–31, https://doi.org/10.1016/j.biomaterials.2016.02.010.
[40] N.C. Tsai, J.W. She, J.G. Wu, P.L. Chen, Y.S. Hsiao, J.S. Yu, Poly(3,4-ethylenedioxythiophene) polymer composite bioelectrodes with designed chemical and topographical cues to manipulate the behavior of PC12 neuronal cells, Adv. Mater. Interfaces 6 (5) (2019), https://doi.org/10.1002/admi.201801576.
[41] L. Juckett, T.M. Saffari, B. Ormseth, J.-L. Senger, A.M. Moore, The effect of electrical stimulation on nerve regeneration following peripheral nerve injury, Biomolecules 12 (12) (2022) 1856, https://doi.org/10.3390/biom12121856.
[42] Q. Wang, Y. Wei, X. Yin, G. Zhan, X. Cao, H. Gao, Engineered PVDF/PLCL/PEDOT dual electroactive nerve conduit to mediate peripheral nerve regeneration by modulating the immune microenvironment, Adv. Funct. Mater. (2024), https://doi.org/10.1002/adfm.202400217.
[43] J. van Bergeijk, K. Haastert, C. Grothe, P. Claus, Valproic acid promotes neurite outgrowth in PC12 cells independent from regulation of the survival of motoneuron protein, Chem. Biol. Drug Des. 67 (3) (2006) 244–247, https://doi.org/10.1111/j.1747-0285.2006.00369.x.